



Effects of alloying elements Mn, Mo, Ti, Si, P and C on the incubation period of void swelling in austenitic stainless steels

Toshimasa Yoshiie¹ · Qiu Xu¹

Received: 3 November 2020 / Revised: 29 December 2020 / Accepted: 29 December 2020 / Published online: 25 March 2021
© The Nonferrous Metals Society of China 2021

Abstract

Void swelling, which induces the degradation of the original properties of nuclear materials under high-energy particle irradiation, is an important problem. The incubation period, a transient stage before the steady void growth, determines the duration of service of nuclear materials. Several experimental studies have been performed on void observations by transmission electron microscopy (TEM), which, however, has a resolution limit for the size of defect clusters. Positron annihilation lifetime spectroscopy (PALS) enables the detection of small vacancy clusters, single vacancies, dislocations and precipitates. The use of these two methods provides complementary information toward detecting defect information in the incubation period. Here, defect structures during the incubation period in austenitic stainless steels, by means of PALS and TEM are reviewed. The role of alloying elements into determining the period is explained. Furthermore, the existing problems and research directions in this field are presented.

Keywords Austenitic stainless steels · Void swelling · Incubation period · Neutron irradiation · Positron annihilation lifetime spectroscopy

1 Introduction

Irradiation in metals by high-energy particles produces point defects, and subsequently, point defect clusters, such as interstitial type dislocation loops and voids. For safe nuclear power plants, overcoming void swelling is essential. Experimental and theoretical analyses reveal the importance of an incubation period as illustrated in Fig. 1, which is a transient period required before steady-state void growth [1–3], such as 1%/dpa (displacement per atom) in austenitic stainless steels [4, 5]. The duration of the incubation period determines the lifetime of the nuclear materials. For this purpose, alloy design has been embraced. However, the experimental results for void swelling in nuclear materials were only limited to the high-dose regime, wherein voids were observed by transmission electron microscopy (TEM). The detection limit of voids by TEM is approximately 1.5 nm in diameter,

which corresponds to 160 vacancies in the case of austenitic stainless steels. Therefore, it is impossible to detect small vacancy clusters and micro-voids that are formed during the incubation period. Herein, the term “micro-voids” refer to unobservable vacancy clusters by TEM. Therefore, there is minimal information available about the behavior of vacancies during this period. Positron annihilation lifetime spectroscopy (PALS) facilitates the detection of vacancy clusters, single vacancies, stacking fault tetrahedra (SFT), precipitates and dislocations [6, 7]. However, it is rather difficult to determine defect cluster types when their lifetimes are similar, owing to the resolution limit of PALS. If the defect size is sufficient, TEM can be employed to identify the nature of defects and geometrical relations between defects, such as voids near grain boundaries. To demonstrate the merits and demerits of both methods, we initially introduce an example of TEM and PALS studies of nickel alloys.

In nickel and nickel alloys irradiated by neutrons to 0.11 dpa at 563 K, voids with well-developed dislocations in nickel and Ni–2at%Ge, and no voids with only small interstitial type dislocation loops in Ni–2at%Si and Ni–2at%Sn were observed by TEM, as shown in Fig. 2 [8]. However, by only TEM, it is unclear whether there exist micro-voids in Ni–2at%Si and Ni–2at%Sn. The results of the PALS of

✉ Toshimasa Yoshiie
yoshiie.toshimasa.3v@kyoto-u.ac.jp

✉ Qiu Xu
xu.qiu.8z@kyoto-u.ac.jp

¹ Institute for Integrated Radiation and Nuclear Science, Kyoto University, Osaka 590-0494, Japan

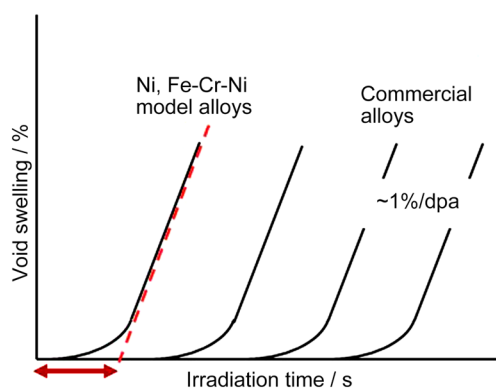


Fig. 1 Relationship between irradiation period and void swelling. The time until the start of swelling as indicated by an allow is an example of the incubation period of model alloys for void swelling

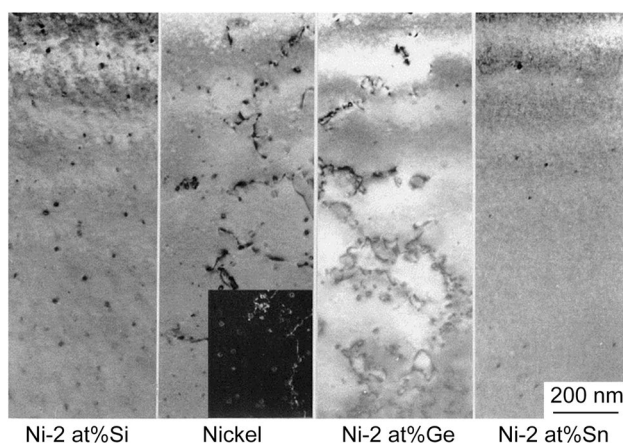


Fig. 2 Damage structures in neutron-irradiated nickel and nickel alloy at 573 K to 0.11 dpa by JMTR. Inset in nickel shows the voids [8]. The magnifications of all photos are the same. Reproduced with permission from Ref. [8]. Copyright 2004 Elsevier

the same specimens are presented in Table 1 [9]. If we can decompose the lifetime into two components, short lifetime τ_1 and long lifetime τ_2 , the latter indicates the existence of defect clusters. Long lifetimes of 464 ps (nickel) and 456 ps (Ni-2at%Ge) evidently show the existence of voids, as depicted in Table 1. The relation between the lifetime and vacancy cluster size is described in the next section. The lifetime is an average and it has a distribution. Usually, if the lifetime exceeds 450 ps, voids are observed by TEM. In

Ni-2at%Si and Ni-2at%Sn, two-component decomposition of lifetime was impossible and the mean lifetime indicated the absence of micro-voids. This result supports the TEM observation presented in Fig. 1. However, when neutron-irradiated nickel at 363 K to a dose of 0.2 dpa was analyzed, micro-voids were detected by PALS, although no voids were observed through TEM as discussed in Sects. 3.2 and 4.1. In this way, PALS is a useful technique for damage structure determination. The disadvantage is the detection limit of cluster concentration. Generally, 100% of the long lifetime intensity I_2 corresponds to a defect concentration of 10^{-4} , and the detection limit is 10^{-7} (the density of approximately 10^{22} m^{-3}). Although in TEM evaluations, the concentration of 10^{-11} (10^{18} m^{-3}) can be observed [10]. As shown in Fig. 3, the geometrical relations between loops and/or voids and grain boundaries are evident. The presence of no interstitial type dislocation loops near grain boundaries in nickel was caused by the escape of loops by one-dimensional motion of them, and loops near grain boundaries in Ni-2at%Sn were the evidence of no one-dimensional motion [8]. Consequently, point defect processes under irradiation can be analyzed, using the grain boundary as the sink of both point defects and their clusters. Therefore, the use of both methods is essential.

Stainless steels are important nuclear materials, but they are vulnerable to void swelling during prolonged neutron-irradiation. Such swelling in neutron-irradiated steel has been studied extensively for many years, mainly by TEM. Therefore, most of studies were conducted after the incubation period. Herein, our studies on defect structures in austenitic stainless steels during the incubation period using PALS and TEM are introduced. We mainly studied titanium-added 316 stainless steel, which was designed for a fusion first wall Japanese primary candidate alloy in the 1980s [11, 12]. Thus there are many irradiation datasets for this alloy, for example, Refs. [10, 13–15], which is referred to as “the Japanese prime candidate alloy (JPCA)” or “Ti-modified 316SS”. The addition of titanium in JPCA is 0.24 wt%. Other differences between type 316SS and JPCA are higher nickel and lower chromium concentration. As molybdenum improves the corrosion resistance and high temperature strength in austenitic alloys, the concentration is the same as that in type 316SS. In our case, however, the alloy composition was the same as JPCA, but we made the heat treatment in our specific manner to compare the effect of

Table 1 PALS of neutron-irradiated nickel and nickel alloys at 573 K to 0.11 dpa [9]

	Ni-2at%Si	Nickel	Ni-2at%Ge	Ni-2at%Sn
Mean lifetime τ_m (ps)	109	251	131	123
Short lifetime τ_1 (ps)	–	115	105	–
Long lifetime τ_2 (ps)	–	464	456	–
Intensity of long lifetime I_2 (%)	–	76	18	–

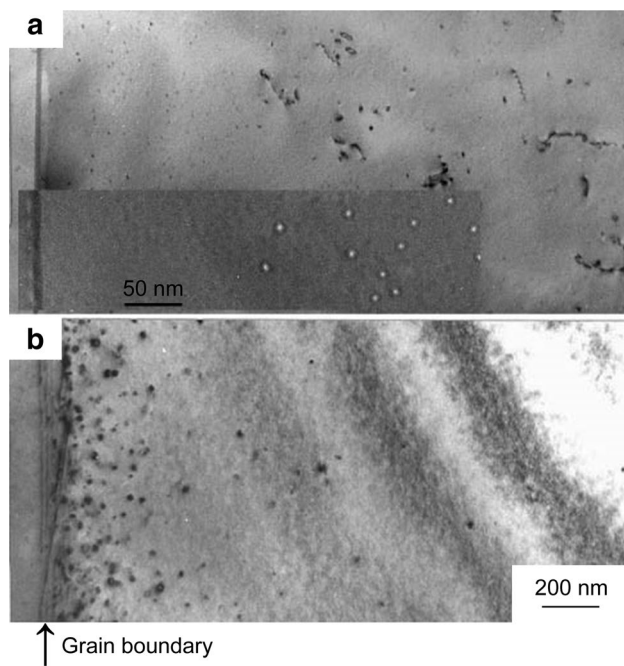


Fig. 3 Damage structures in **a** neutron-irradiated nickel and **b** Ni-2at%Sn near grain boundaries at 573 K to 0.11 dpa by JMTR. Note that the magnification of the photo inserted in **a** is different

alloying elements as described in the following section, and we herein refer to it as “Ti-added modified 316SS”.

Recently, austenitic stainless steels have been rather unpopular for high-dose nuclear materials because of the nickel-containing face-centered cubic structure, which causes higher swelling than the body-centered cubic structure, and helium production from nickel through nuclear reactions. For example, tungsten is expected for the fusion reactor divertor material, and ferritic stainless steels for the first wall materials. However, austenitic alloys have received considerable attention as a beam window material for

spallation neutron sources [16, 17] and accelerator-driven systems [18]. Several studies have been conducted to investigate the effect of alloying elements on void swelling in JPCA, for example, Refs. [19, 20]. In the present study of damage structures during the incubation period of austenitic stainless steels, two series of experiments were performed: (1) the addition of one alloying element in the Fe–Cr–Ni ternary alloy in Sect. 3.1, and (2) the successive addition of alloying elements to the Fe–Cr–Ni ternary alloy in Sect. 3.2. For this study, not only commercial alloys such as SUS316SS, but also nickel and model austenite alloys were employed. The use of nickel is considered to be the simplest model of an austenitic alloy. Irradiation experiments were performed using neutrons and electrons.

2 Experimental

The specimens used are listed in Table 2 [21–23]. Herein SUS316L (E), SUS316 (F), SUS304(G) and Ti-added modified 316SS (J) present practical austenitic stainless steels. Model alloys, FeCrNi, FeCrNiP, FeCrNiTi, ‘A’, ‘B’, ‘C’ and ‘D’ were prepared based on the composition of Ti-added modified 316SS. For the specimen preparation, all the specimens including pure nickel (Ni) were first cold-rolled to a thickness of 0.1 mm and punched out into 3 mm-diameter disks for TEM studies and 5 mm-diameter disks for PALS evaluations, and annealed at 1173 K in vacuum for 1 h followed by air-cooling. Under this condition, no precipitates were observed in all the alloys by TEM observation.

Electron-irradiation was performed using an electron linear accelerator at the Institute for Integrated Radiation and Nuclear Science, Kyoto University with an acceleration voltage of 30 MV. Another electron irradiation was performed by a high-voltage TEM at Osaka University with an acceleration voltage of 2 MeV. Neutron irradiation was

Table 2 Composition of specimens [21–23]

Specimen	Composition (wt%)
Ni	Pure nickel (purity 99.999%)
Fe–15Cr–16Ni	Fe–15.0Cr–16.0Ni
FeCrNi	Fe–16.05Cr–16.69Ni–0.0043C
FeCrNiP	Fe–15.23Cr–17.02Ni–0.09P–0.001C
FeCrNiTi	Fe–15.48Cr–16.93Ni–0.18Ti–0.0016C
‘A’	Fe–16.08Cr–16.64Ni
‘B’	Fe–15.35Cr–15.88Ni–1.89Mn–2.67Mo
‘C’	Fe–15.39Cr–15.8Ni–1.88Mn–2.66Mo–0.53Si
‘D’	Fe–15.39Cr–15.92Ni–1.89Mn–2.68Mo–0.53Si–0.24Ti
E (SUS316L)	Fe–17.35Cr–12.05Ni–0.85Mn–2.08Mo–0.47Si–0.019C–0.027P–0.001S
F (SUS316)	Fe–19.22Cr–12.58Ni–1.82Mn–2.26Mo–0.39Si–0.05C–0.019P–0.004S
G(SUS304)	Fe–18.12Cr–9.08Ni–0.85Mn–0.48Si–0.05C–0.027P–0.0025S
J (Ti-added modified SUS316)	Fe–15.27Cr–15.8Ni–1.88Mn–2.66Mo–0.53Si–0.24Ti–0.055C–0.024P

performed with fission neutrons using the experimental fast reactor JOYO and the Japan Materials Testing Reactor (JMTR) of the Japan Atomic Energy Research Institute, the Materials Open Test Assembly of the Fast Flux Test Facility (FFTF/MOTA) in the USA, Belgian Reactor 2 (BR-2) of the Belgian Nuclear Research Center, the temperature control irradiation facility of the research reactor of Kyoto University (KUR) [24], and with 14 MeV D-T neutrons by the Rotating Target Neutron Source II (RTNS-II) of Lawrence Livermore National Laboratory in the USA.

The TEM evaluation was performed using a 200 keV JEOL 2010. Three types of point defect clusters, dislocation loops, SFT and voids, were observed by TEM. Loops were confirmed by inside/outside methods [25] when the size was enough, and all the loops examined were the interstitial type. SFT were identified by their triangle shapes observed from $\langle 110 \rangle$ and $\langle 111 \rangle$ directions of the matrix of specimens. Voids was confirmed by void images.

The PALS of the specimens was measured at room temperature using Na-22 and a conventional fast-fast spectrometer with a time resolution of 190 ps (full width at half maximum) in the Institute for Integrated Radiation and Nuclear Science, Kyoto University, and each spectrum was accumulated to a total of 1×10^6 counts. The maximum positron energy emitted from Na-22 is 540 keV and the average is 180 keV. The penetration depth of positrons before annihilation is about 0.01 cm in the case of nickel and iron. In this study, irradiations were performed by neutrons and electrons, and defects were formed homogeneously in the matrix of specimens, and the detection of defect clusters was possible. When positrons are injected into a perfect metal lattice, they mainly annihilate with free electrons in the lattice in a short time (bulk positron lifetime). If defects exist, positrons reside in them and annihilate less rapidly than in the bulk of no defects depending on the size and nature of defects (defect positron life time). The positron lifetime spectra were analyzed using the PALSfit program [26]. By the two-component analysis or the three-component analysis, the main two or three lifetimes are obtained. Usually in the two-component analysis of irradiated metals, the long lifetime and the short lifetime components refer to the vacancy clusters and the bulk of no defect area, respectively. But there is a case that the long lifetime and short lifetime refer to large micro-voids and small micro-voids, respectively. In this case the bulk positron lifetime component is omitted because of low annihilation rate of positrons at the bulk. The mean lifetime is the average of two or three components.

The positron annihilation lifetimes depend on the composition of the alloying elements; however, in austenitic stainless steels, the effect is small. We only calculated the lifetime of the mono-vacancy in Fe–14Cr–13Ni. The lifetimes of the matrix and single vacancy were 106 ps and 183 ps, respectively [27] and it was approximately the same as that in nickel. Therefore, we adopted the lifetime of nickel [28, 29] for the austenitic alloys, as depicted in Table 3. V_1 and V_n represent the single vacancy and micro-void of n vacancies, respectively. S_m is the SFT of m vacancies. SFT are special defects, and SFT of 0.5 nm on one side of the tetrahedron was observed in the nickel alloy by TEM [30]. Kuramoto et al. [29] also calculated the lifetime of dislocations and dislocations with vacancies in nickel. The lifetimes were between the mono-vacancies and the matrix, depending on the configuration in nickel. The lifetime of precipitates is mainly caused by the interface between the precipitates and the matrix, and we usually assume it to be between 140 and 150 ps. Prior to irradiation, the lifetimes of all the specimens used ranged from 107 to 110 ps and two-component analysis was impossible.

3 Effect of alloying elements

Alloying elements affect the damage structures and consequently void swelling. In general, undersized elements such as silicon and phosphorus in austenitic stainless steels interact with interstitials, and oversized elements titanium, manganese and molybdenum interact with vacancies by their strain fields, and reduce the mobility of point defects. In Sect. 3.1, the role of alloying elements was studied by TEM analysis. In this case, neutron-irradiation was performed by means of a special irradiation mode, which was the cyclic-temperature neutron-irradiation between low and high temperatures [21, 31] in addition to the normal constant-temperature irradiation. The cyclic-temperature irradiation facilitates the detection of point defect processes during irradiation. In Sect. 3.2, the detection of micro-voids by PALS during the incubation period was demonstrated.

3.1 Detection of the role of titanium and phosphorus through cyclic-temperature neutron-irradiation

The effects of phosphorus and titanium on the microstructural evolution, especially void nucleation and growth in an

Table 3 Relation between lifetimes and the size of vacancy clusters in nickel. V_n : micro-voids of n vacancies, S_m : SFT of m vacancies [28, 29]

Size of V clusters	V_1	V_2	V_5	V_{13}	V_{19}	V_{43}	V_{79}	S_3	S_{10}	S_{21}	S_{28}
Lifetime (ps)	176	195	264–297	341	371	410	427	183	170	155	130

austenitic stainless steel model alloy FeCrNi were investigated using the JMTR with improved temperature control [21, 32]. As shown in the upper photographs in Fig. 4, interstitial type dislocation loops were observed in the ternary model alloy FeCrNi irradiated at 473, 573, 623, and 673 K, respectively. Notably, SFT were observed in the specimens irradiated below 623 K, whereas voids were only observed at temperatures higher than 573 K. The density and size of the dislocation loops and voids were temperature dependent. The dislocation loop and void density decreased, while the dislocation loop and void size increased with irradiation temperature. From the dislocation loop size distributions, it was found that the nucleation of dislocation loops at 673 K occurred continuously during irradiation, whereas at the lower temperatures it was near-complete at the early irradiation stage. No spatial relationships between voids and other defects were recognized. Void swelling was 0.13% at 673 K.

The effect of the addition of titanium and phosphorus was compared, as presented in Figs. 5, 6, 7 [31]. No voids were observed in the 0.1P-added alloy, FeCrNiP (Fig. 6), and most of the observable defects were not dislocation loops but needle-shaped precipitates identified as the phosphides Fe_2P . The addition of titanium, FeCrNiTi as shown in Fig. 7, marginally suppressed void formation relative to that without titanium, FeCrNi as shown in Fig. 5.

To investigate the role of phosphorus and titanium on microstructural evolution in the model alloy FeCrNi, neutron-irradiation with cyclic-temperature was performed.

Figure 5 (right) shows the typical damage microstructures formed in FeCrNi irradiated at 473/673 K with six cycles (total dose of 0.13 dpa). In FeCrNi, interstitial and vacancy defect clusters are easily formed [31]. As shown in the upper photographs in Fig. 5, small dislocation loops with high density and SFT were homogeneously formed in the matrix at 473 K, while large dislocation loops and voids were formed at 673 K. According to these results, it can be expected simply that intermediate microstructures between 473 and 673 K appear in the 473/673 K cyclic irradiation. However, the formation of dislocation loops was suppressed strongly, and similarly, the formation of voids was also suppressed in the cyclic-temperature irradiation as shown in the lower right photograph presented in Fig. 5. Notably, little damage remained in the 473/673 K-irradiation.

Figure 6 shows the damage microstructures in FeCrNiP irradiated under the same conditions, as FeCrNi is shown in Fig. 5. Fe_2P precipitates were also formed during the cyclic-temperature irradiation, although their nucleation was suppressed. The size of precipitates produced in 473/673 K-irradiation was larger than that in 673 K-irradiation. As shown in the lower photographs of Fig. 6, no significant difference in void swelling was observed in 473/673 K-irradiation compared with the constant-temperature irradiation. The phosphorus concentration was 0.024 wt% in JPCA, and there were no differences in void formation between the two alloys with phosphorus addition of 0.024 wt% and 0.1 wt%. No voids were also observed at 573 K, 673 K and

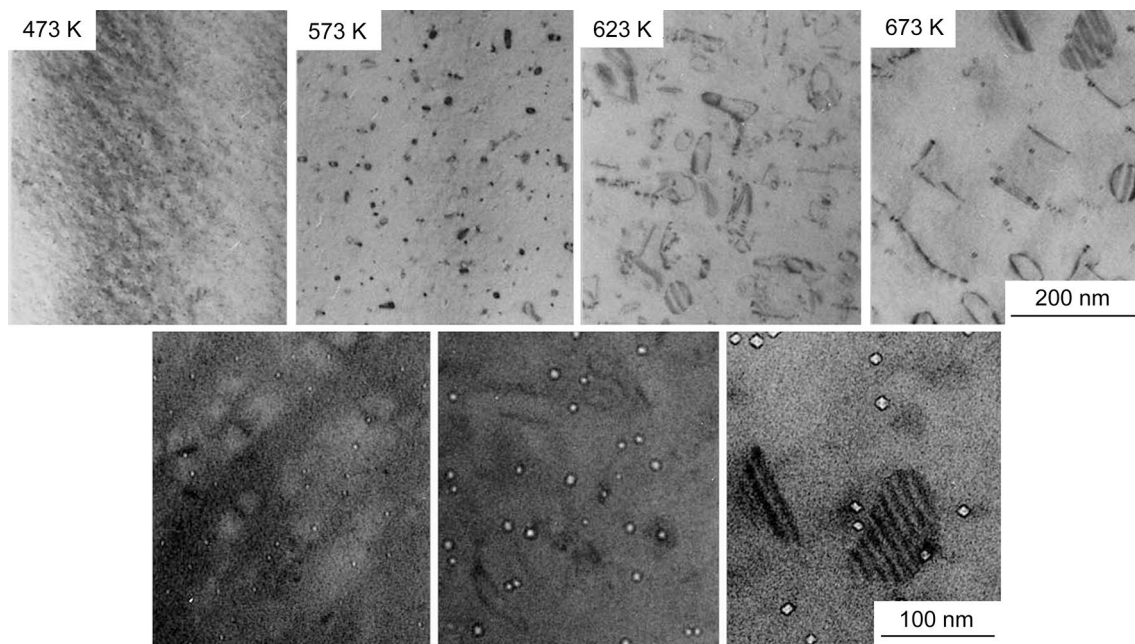


Fig. 4 Typical damage structure in FeCrNi irradiated by JMTR at 473 K (0.037 dpa), 573 K (0.054), 623 K (0.16) and 673 K (0.14). Upper photos are bright-field images and lower photos are void

images at the corresponding temperature. The magnifications of upper four photos and lower two photos are the same. Reproduced with permission from Ref. [21]. Copyright 1992 Elsevier

Fig. 5 Typical damage structure in FeCrNi irradiated by JMTR at 473 K (0.13 dpa), 673 K (0.037) and cyclic-temperature at 473 K/673 K with six cycles (0.13). Upper photos are bright-field images (B.F.), and lower photos are dark-field image (D.F.) and void image (V.E.), respectively. The magnifications of all photos are the same. Reproduced with permission from Ref. [31]. Copyright 1994 Elsevier

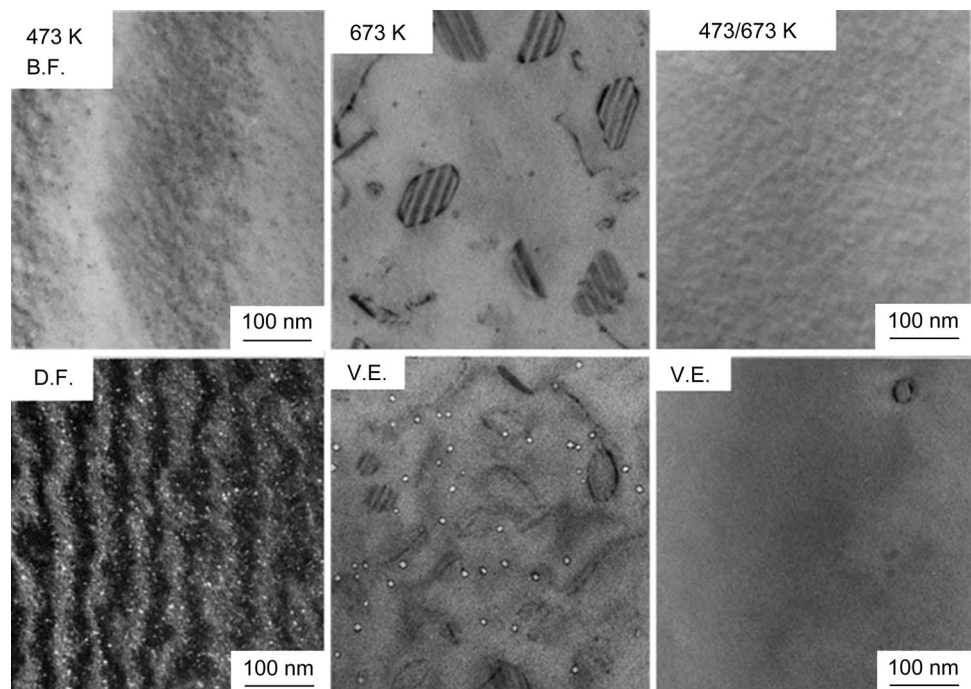
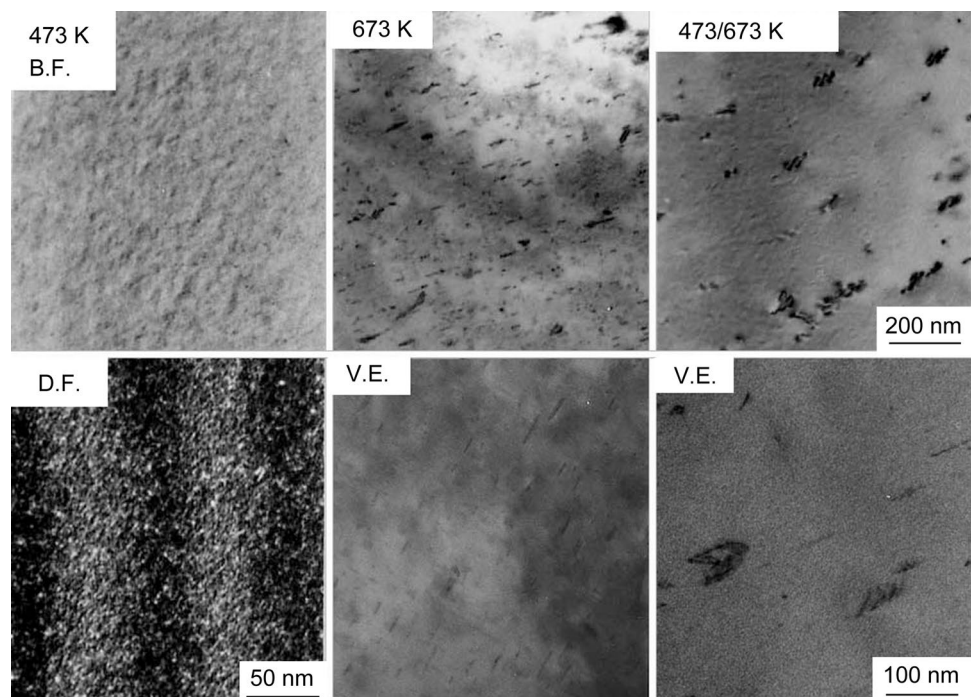


Fig. 6 Typical damage structure in FeCrNiP irradiated by JMTR at 473 K (0.13 dpa), 673 K (0.037) and cyclic-temperature at 473 K/673 K with six cycles (0.13). Upper photos are bright-field images (B.F.), and lower photos are dark-field image (D.F.) and void image (V.E.), respectively. The magnifications of left two photos, upper right two photos and lower right two photos are the same. Reproduced with permission from Ref. [31]. Copyright 1994 Elsevier

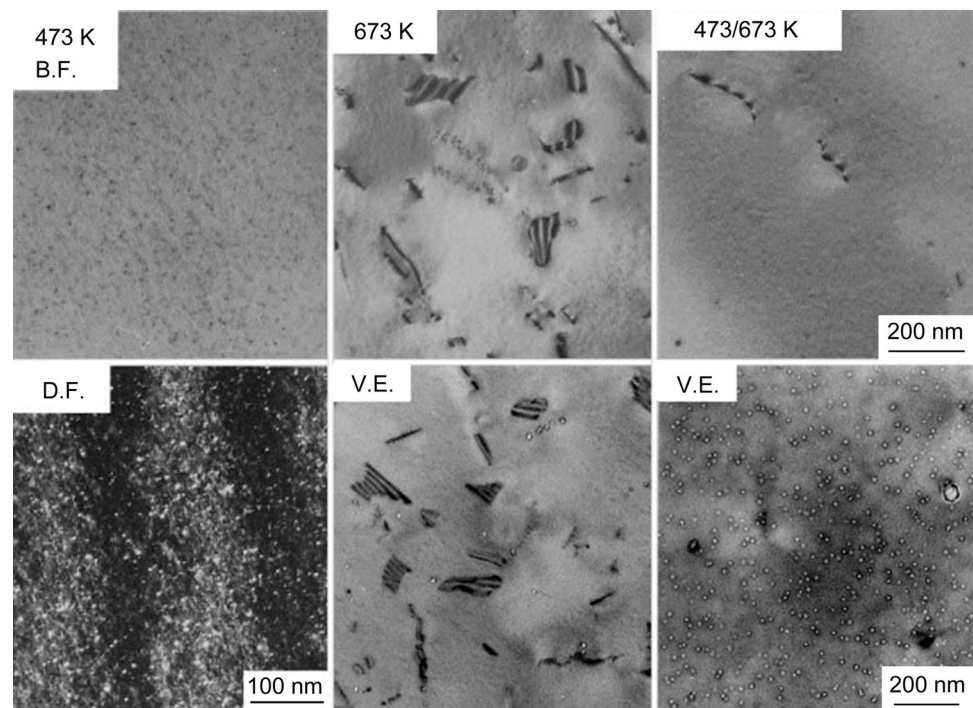


473/673 K-irradiation in Fe–15.8Cr–16.9Ni–0.024P similar to FeCrNiP, although the density of precipitates was low while that of loops was high relative to FeCrNiP [21]. The damage microstructures formed in titanium-added alloy FeCrNiTi irradiated at 473, 673 and 473/673 K are illustrated in Fig. 7. The formation of dislocation loops was suppressed in the cyclic-temperature irradiation; however, a

high density of small voids (3–10 nm) were formed. In FeCrNiTi, compared with the constant-temperature irradiation at 673 K, whose void swelling was estimated to be 0.04%, the void swelling of the cyclic-temperature 473/673 K-irradiation was 1.5%.

Numerical analyses of defect reaction processes during neutron-irradiation at cyclic-temperatures were carried out

Fig. 7 Typical damage structure in FeCrNiTi irradiated by JMTR at 473 K (0.13 dpa), 673 K (0.037) and cyclic-temperature at 473 K/673 K with six cycles (0.13). Upper photos are bright-field images (B.F.), and at lower photos are dark-field image (D.F.) and void image (V.E.), respectively. The magnifications of left two photos and right four photos are the same. Reproduced with permission from Ref. [31]. Copyright 1994 Elsevier



based on the rate theory [21, 31]. The calculated results show that vacancy-rich conditions appear temporarily just after changing the temperature from low to high due to the movement of the high density of single vacancies produced by irradiation at low temperatures, and the decomposition of small vacancy clusters formed at low temperatures by reacting with interstitials produced at high temperatures. If mobile interstitial clusters are trapped at low temperatures, they can escape from the trapping site and also contribute to the annihilation of vacancy clusters. Consequently, the growth of both interstitial and vacancy clusters is prevented, as evident for FeCrNi.

No void formation in FeCrNiP is easy to understand. Although, the density of Fe_2P decreases while the size increases by the cyclic-temperature irradiation compared with that at the 673 K-irradiation. The Fe_2P clusters are sufficient in numbers to act as a sink for interstitials and vacancies, and prevent void formation.

Titanium is an oversized element of 37% in austenitic stainless steels [33] and has a strong binding with vacancies and their clusters. The interaction of titanium with vacancies reduces the formation of voids by the constant-temperature irradiation. The dilatational stress field near the vacancy clusters decreases by the absorption of titanium. When the temperature is changed from low to high, the reduced dilatational stress field prevents the absorption of interstitials and their clusters. Subsequently, the growth of voids is promoted in cyclic-temperature irradiated FeCrNiTi.

3.2 Effects of successive addition of alloying elements on micro-void formation

Here, alloying elements were increased to approach JPCA, in our case Ti-added modified 316SS (J), using alloys 'A', 'B', 'C' and 'D', and the effect of successive addition of elements was studied after electron-irradiation and neutron irradiation.

3.2.1 PALS of electron-irradiated austenitic alloys

The damage structure evolution was studied by 30 MeV electron-irradiation at 343 K to a dose of 1.2×10^{-2} dpa, as shown in Fig. 8a. The effect of the alloying elements was not clear. The result of the two-component analysis shows the existence of vacancies and micro-voids of a few vacancies in Ni. Other alloys contained only single vacancies. By 573 K-irradiation at a dose of 1.5×10^{-3} dpa, the effect of the alloying elements was clearly observed, as shown in Fig. 8b. In Ni, the main defects were SFT and loops. In 'A', 'B' and 'C', small micro-voids were formed. In 'D' and four practical alloys, 'J', 'E', 'F' and 'G', the two-component analysis was impossible and the lifetimes were just the same as those before irradiation. The effects of silicon (alloy 'C') and titanium ('D') were detected by the 573 K-irradiation.

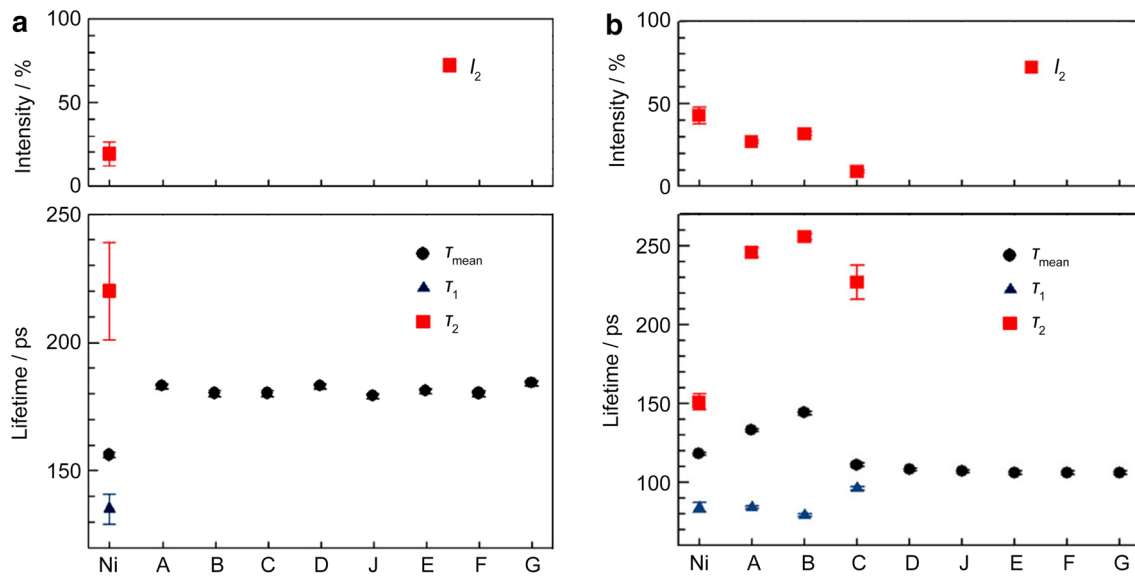


Fig. 8 PALS of 30 MeV electron-irradiated Ni, model alloys and commercial alloys of austenitic stainless steels at **a** 343 K to a dose of 1.5×10^{-2} dpa and **b** 573 K to 1.5×10^{-3} dpa. τ_{mean} is the mean

lifetime, and τ_1 , τ_2 , I_2 are the short lifetime, the long lifetime and the intensities of the long lifetime component, respectively. Reproduced with permission from Ref. [22]. Copyright 2013 Elsevier

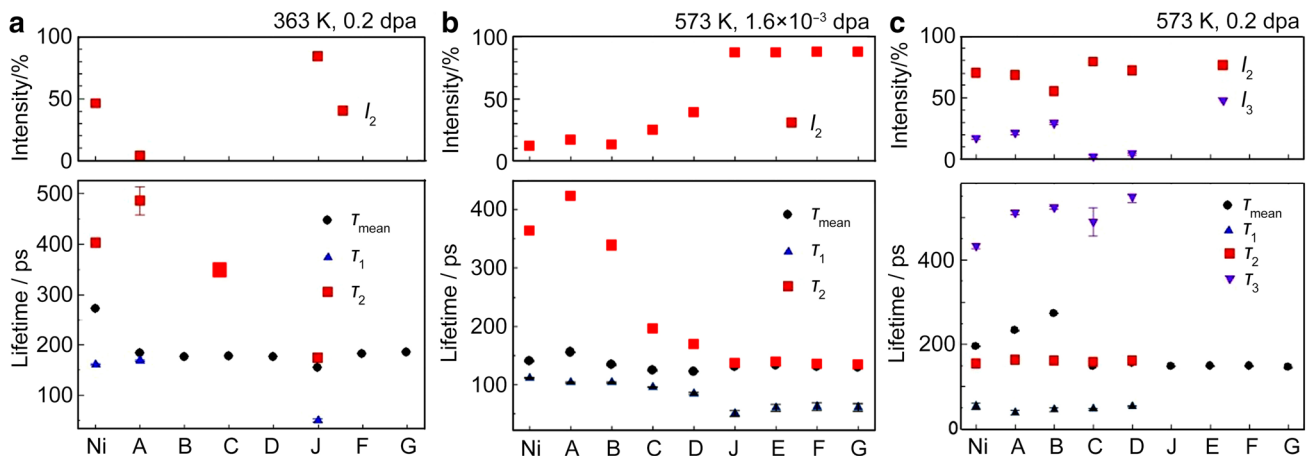


Fig. 9 Positron annihilation lifetimes of neutron-irradiated Ni, model alloys and commercial austenitic stainless steels at **a** 363 K to a dose of 0.2 dpa by BR-2, **b** 573 K to 1.6×10^{-3} dpa by KUR, and **c** 573 K to 0.2 dpa by BR-2. τ_{mean} is the mean lifetime, and τ_1 , τ_2 and I_2 are

the short lifetime, long lifetime and the intensity of the long lifetime, respectively. τ_3 and I_3 are the result of three-component analysis of PALS. Reproduced with permission from Ref. [22]. Copyright 2013 Elsevier

3.2.2 PALS of fission neutron-irradiated austenitic alloys

PALS of fission neutron-irradiated austenitic alloys [22] including Ni at 363 K and 573 K are illustrated in Fig. 9. The results are similar to those of electron-irradiation. The existence of voids was detected in Ni and ‘A’ after the 363 K-irradiation (Fig. 9a). Other alloys only showed the existence of mono-vacancies and/or SFT and dislocation loops. At the 573 K low dose irradiation (Fig. 9b) in Ni, ‘A’, ‘B’, ‘C’ and ‘D’, the micro-voids and/or vacancies were detected. The

long lifetimes of ‘C’ and ‘D’ were low, which were attributed to the effects of silicon and titanium. In carbon-containing alloys, ‘E’, ‘F’, ‘G’ and ‘J’, no existence of micro-voids was detected. The lifetimes corresponded to SFT, loops or precipitates. The effect of carbon was clearly demonstrated by high-dose irradiation at 573 K (Fig. 9c). Very low density of micro-voids formation in silicon (‘C’) and titanium (‘D’) addition, and no micro-voids in carbon including alloys (‘E’, ‘F’, ‘G’ and ‘J’) were detected. Although the lifetime of carbon-containing alloys corresponded to that of SFT, loops

and precipitates, the drastic change due to the addition of carbon led us to conclude that the main defects were metal carbides. We will discuss this point in Sect. 5.2.

4 Damage structures in Ti-added modified 316SS

Most of the studies on damage structure in JPCA were performed at high temperatures and high irradiation doses [4, 10, 13–15, 34–37]. The main interest entailed the formation of voids and precipitates. In this section, the damage structures in Ti-added modified 316SS from low to high temperatures and from low to high doses are presented.

4.1 Temperature dependence studied by TEM and PALS

The damage structure changes with irradiation temperatures as well as the alloy concentration, as discussed in Sect. 3.2. Figure 10 shows the neutron-irradiation temperature dependence of defect structures in Ti-added SUS316 [23]. The results of Ni and Fe–15Cr–16Ni are also presented for comparison. The damage structures of Ni and Fe–15Cr–16Ni are almost the same. At low temperatures, SFT and interstitial

type dislocation loops are observed, and at high temperatures, voids are observed. These results support the results of PALS discussed in Sect. 3.2.2. However, in Ti-added modified 316SS, very fine defects are observed [23], and only at 573 K, the number density of SFT and loops were estimated. Below 573 K, defect clusters were very fine and above 573 K their densities were too low to estimate. The images of the SFT and loops are shown by 14 MeV neutron-irradiation and fission neutron-irradiation, respectively, in Fig. 11. The left-hand photograph of Fig. 11 was taken of the thin foil irradiation, where the specimen was thinned before irradiation [38], and the dark-field weak-beam observation. By thin foil irradiation, the triangular-shaped SFT are observed because of the easy escape of interstitials, and SFT were formed directly during cascade collapse. As shown in the dark-field image of the right-hand photograph in Fig. 11, interstitial type dislocation loops are observed as two dots along the diffraction vector g . The lines of no contrast are perpendicular to g with $g \times b = 0$, which is the evidence of loops [25].

Figure 12 shows the temperature dependence of defect structures in 14 MeV neutron-irradiated Ti-added modified 316SS. The temperature dependence was quite low until 823 K. In order to get information on the defect structure change between irradiations at low temperature and high

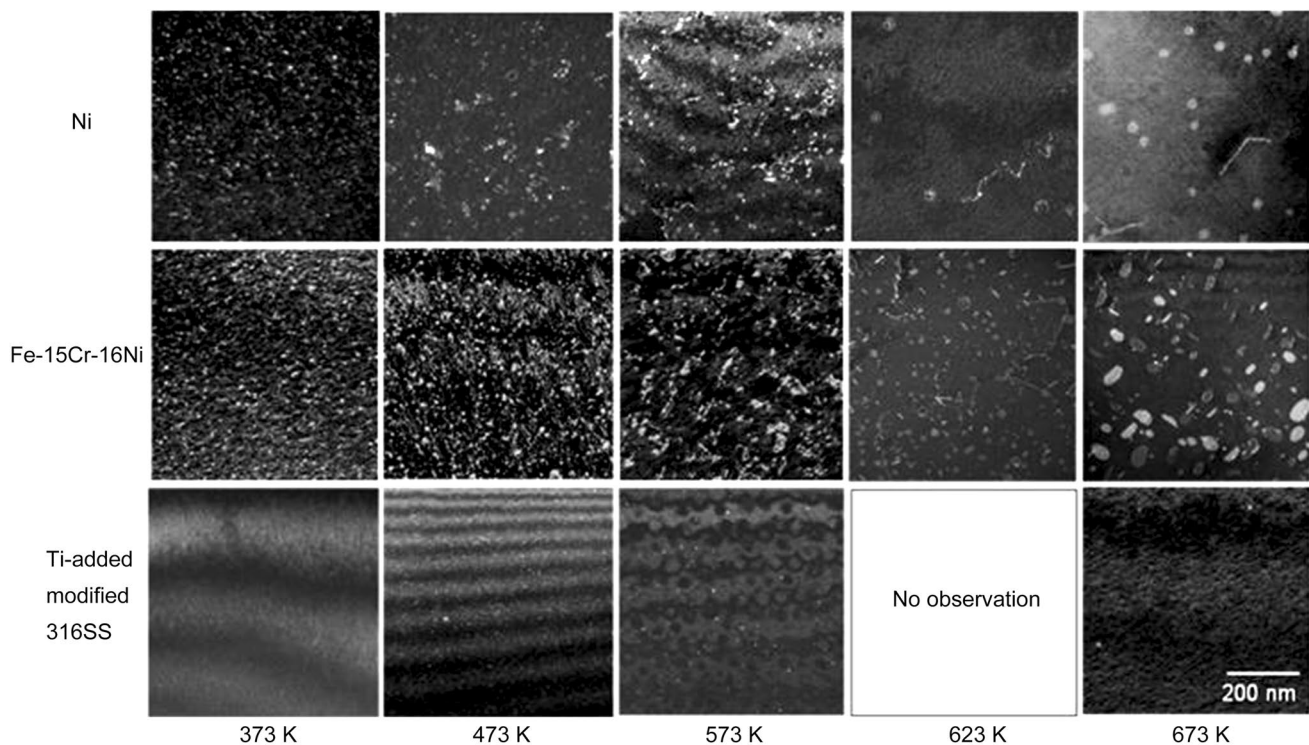


Fig. 10 Irradiation temperature dependence of defect structures in Ni, Fe-15Cr-16Ni and Ti-added modified 316SS, irradiated by JMTR at 373 K (0.33 dpa), at 473 K (0.08), at 573 K (0.11), 623 K (0.33),

and 673 K (0.29). The magnifications of all photos are the same. Reproduced with permission from Ref. [23]. Copyright 2013 Taylor & Francis

Fig. 11 14 MeV neutron-irradiated Ti-added modified 316SS as thin foil irradiation at 423 K to a dose of 5×10^{-3} dpa (left) by RTNS-II and fission neutron-irradiated Ti-added modified 316SS at 573 K to a dose of 0.11 dpa (right-side two photos) by JMTR. The magnifications of right two photos are the same

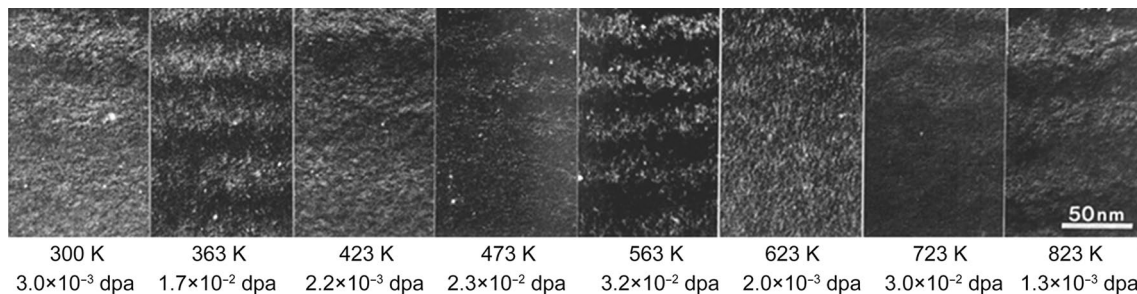
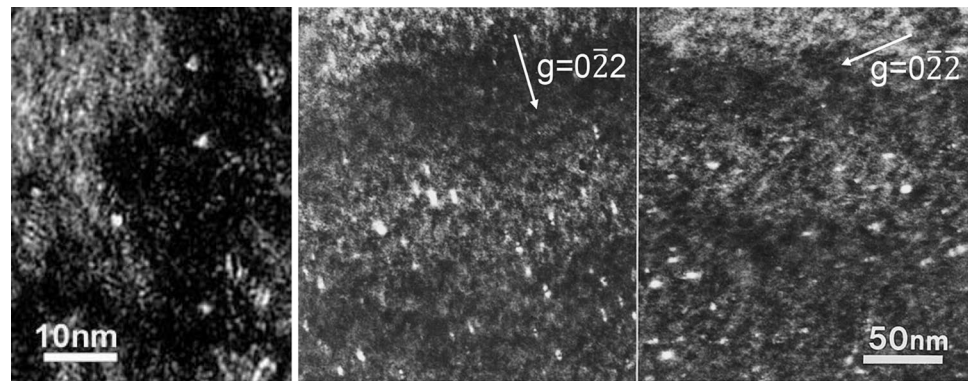


Fig. 12 Temperature dependence of damage structures of 14 MeV neutron-irradiated Ti-added modified 316SS by RTNS-II. The magnifications of all photos are the same

temperature, PALS was performed on 14 MeV neutron-irradiated Ti-added modified 316SS at various temperatures as shown in Fig. 13 [27]. At low temperatures, the lifetime corresponded to single vacancies and vacancy clusters of a few vacancies. Above 623 K, no defects were detected.

The irradiation dose dependences of PALS at 363 K and 563 K are shown in Fig. 14. By 363 K-irradiation (Fig. 14a), the long lifetime did not change from the low dose and only the intensity increased, which means that the concentration of the single vacancies increases. By 563 K-irradiation (Fig. 14b), the long lifetime increased and the intensity did not change significantly with the irradiation dose, which indicated the growth of defects. One possible explanation is the growth of metal carbides, as discussed in the next section.

The annealing behavior of 30 MeV electron-irradiated Ti-added modified 316SS at 100 K is shown in Fig. 15. The mean lifetime decreased from 473 K and almost recovered at 623 K. The annealing of 14 MeV neutron-irradiated nickel at 293 K was performed in TEM. The number of the total clusters also started to decrease from 473 K and only few remained at 623 K [39]. In the Ni case, clusters were interstitial type dislocation loops and SFT. In the low temperature electron-irradiated Ti-added modified 316SS, the formation of the same defect clusters is expected. The instability of SFT and loops above 473 K and decrease of mean lifetime

above 473 K-irradiation (Fig. 13) support our conclusion in Sect. 3.2.2 that the main defect clusters are metal carbides in carbon-containing alloys above 573 K.

4.2 Defect structures at high dose

In Ti-added modified 316SS, large defects were not observed by TEM at a dose of 0.11 dpa. Only small loops and SFT were observed as shown in Figs. 10, 11 and 12. After irradiation at 673 K–4.2 dpa, loops and precipitates (metal carbides) were observed. By irradiation at 763 K–4.2 dpa and at 873 K–0.47 dpa, only precipitates were observed as shown in Fig. 16 [27]. By PALS of high-dose irradiation, the existence of micro-voids was detected above 4.2 dpa as shown in Fig. 17 [27]. Even after irradiation of 15 dpa at 701 K, the micro-void size was almost 10 vacancies. The result of electron-irradiation by high-voltage TEM is shown in Fig. 18. After the growth of interstitial type dislocation loops and tangling of dislocations, voids were formed at a dose of 18.5 dpa.

Many neutron-irradiation studies were carried out using JPCA. The void swelling at high doses is listed in Table 4. We only selected the result of the solution-annealed JPCA. In addition, the high-dose data presented in this work were added, which was obtained from the positron diffusion model [40, 41]. In Table 4, the data are scattered, but in

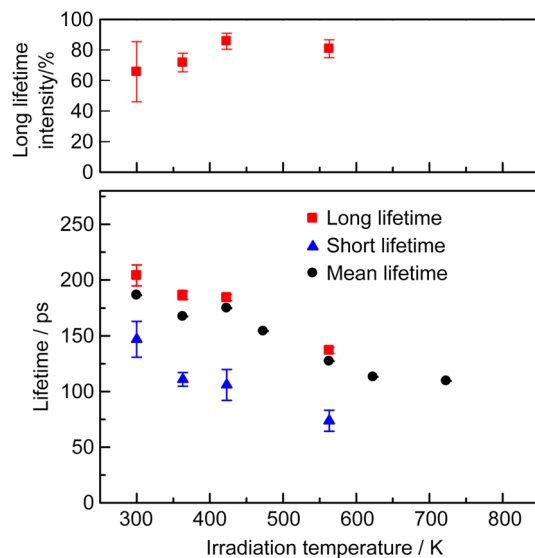


Fig. 13 Irradiation temperature dependence of defect structures in 14 MeV neutron-irradiated Ti-added modified 316SS to doses of 10^{-3} – 10^{-2} dpa by RTNS-II. Reproduced with permission from Ref. [27]. Copyright 2011 Elsevier

general at low doses, the number density of voids is high and void size is small. Using irradiation doses between 34 and 37 dpa in the High Flux Isotope Reactor (HFIR) at the Oak Ridge National Laboratory, even at 573 K, 0.23% swelling (33.6 dpa) was observed and the highest amount of swelling was 0.51% (34.5 dpa) at 773 K [14]. Kato et al. [15] reported void swelling of 0.078% (34.7 dpa) and 7.64% (57.8 dpa) during irradiation at 793 K by FFTF/MOTA. If the

incubation dose is defined as the cumulative dose required to reach a swelling of 1%, and then the value for JPCA is approximately 50 dpa at 793 K.

5 Damage structures during incubation period

The effect of alloying elements was detected on void and/or micro-void formation as mentioned above. The role of alloying elements was divided into two categories. One is the interaction of alloying elements with point defects and their clusters, which reduces the mobility of them. The interaction is caused by the microscopic strain field around alloying elements. The other is the formation of precipitates, which promotes the mutual annihilation of point defects.

5.1 Interaction of alloying elements with point defects

Under electron-irradiation at 343 K to a dose of 1.5×10^{-2} dpa (Fig. 8a), vacancy clusters were formed only in Ni. In other alloys, only single vacancies were detected. Under neutron-irradiation at a temperature of 363 K to a dose of 0.2 dpa (Fig. 9a), micro-voids were formed in Ni and ‘A’ (Fe–Cr–Ni), but only single vacancies were formed in the other alloys just the same as low dose electron irradiation. Although micro-voids were formed in Ni and ‘A’, the intensity of long lifetime l_2 , which presented the ratio of positrons annihilated at micro-voids, indicated that the density

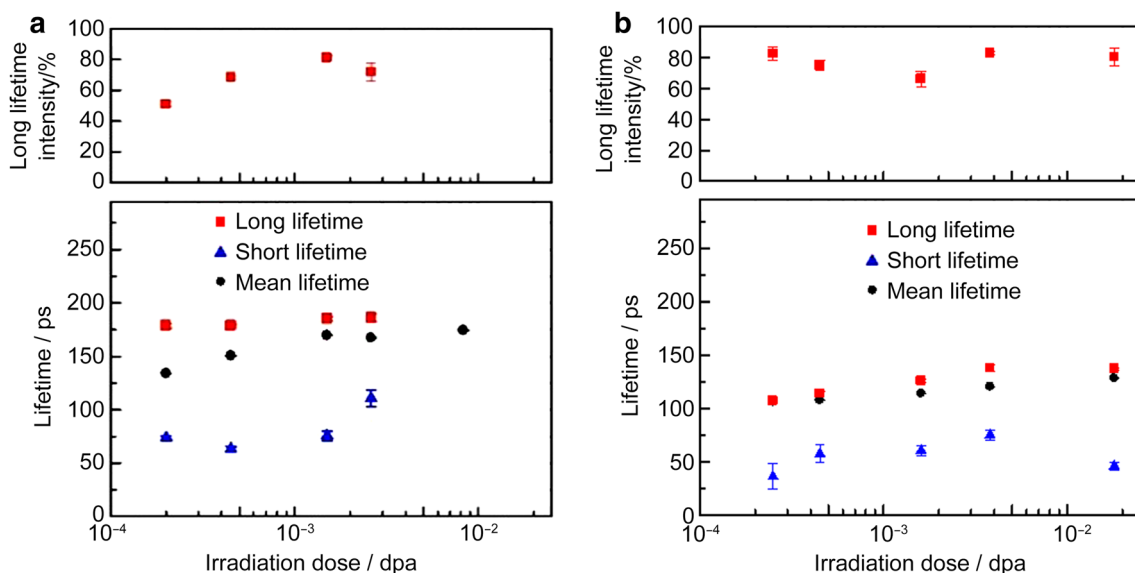


Fig. 14 Irradiation dose dependence of defect structures in 14 MeV neutron-irradiated Ti-added modified 316SS at **a** 363 K and **b** 563 K by RTNS-II. Reproduced with permission from Ref. [27]. Copyright 2011 Elsevier

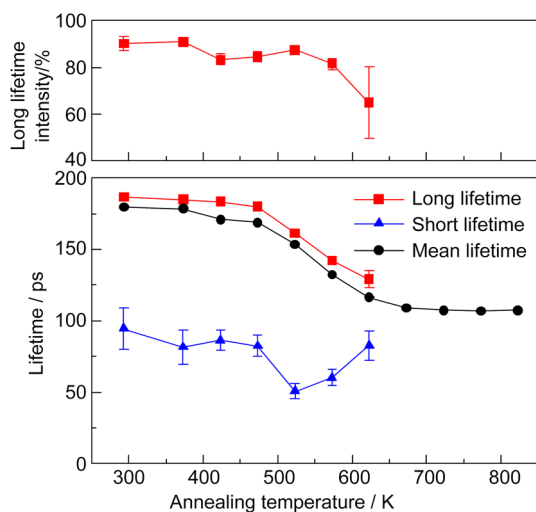


Fig. 15 Annealing behavior of 30 MeV electron-irradiated Ti-added modified 316SS to a dose of 1.4×10^{-3} dpa at 100 K. Reproduced with permission from Ref. [27]. Copyright 2011 Elsevier

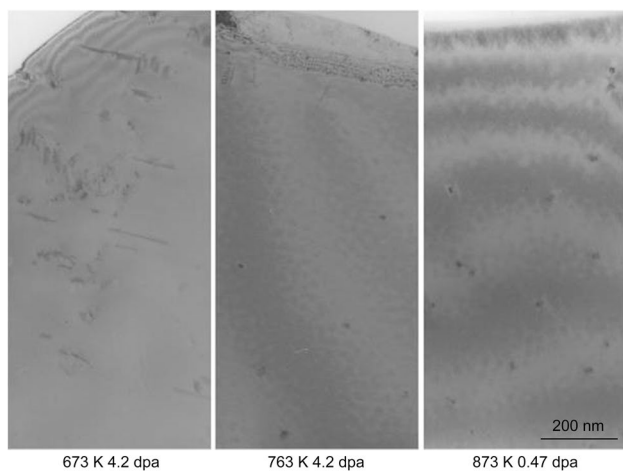


Fig. 16 Defect structures of fission neutron-irradiated Ti-added modified 316SS by JOYO. The magnifications of all photos are the same. Reproduced with permission from Ref. [27]. Copyright 2011 Elsevier

of micro-voids in 'A' was very low compared with that of Ni. These are effects of chromium which is an oversized element in Fe–Cr–Ni alloys [42]. Manganese and molybdenum are also oversized and interact with vacancies. The trapping of point defects reduces the nucleation and growth of micro-voids [43]. Under neutron-irradiation at a temperature of 573 K to a dose of 1.6×10^{-3} dpa (Fig. 9b), micro-voids were formed in Ni, 'A' and 'B' ('A' + Mn + Mo). With an increased dose of 0.2 dpa, micro-voids were formed even in 'C' ('B' + Si) and 'D' ('C' + Ti), although the concentration of micro-voids was low as indicated by I_3 in Fig. 9c. These results indicate that the addition of silicon and

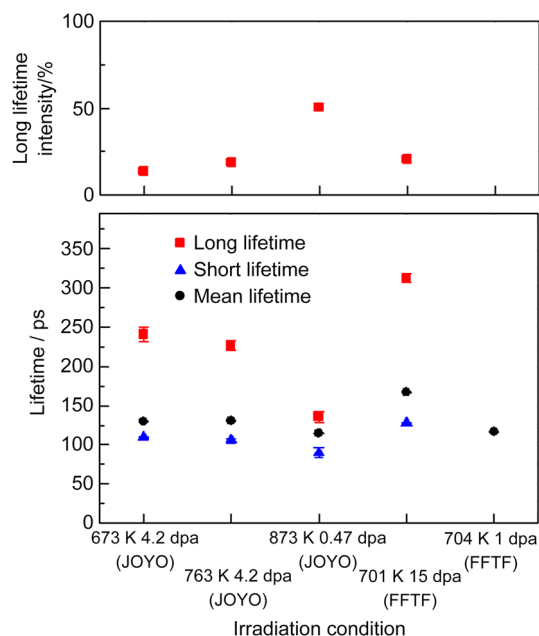


Fig. 17 PALS of neutron-irradiated Ti-added modified 316SS at high temperature and high dose. Reproduced with permission from Ref. [27]. Copyright 2011 Elsevier

titanium prevented micro-void formation. The influence of an undersized element, silicon, in austenitic stainless steels on swelling occurs by many mechanisms [44]. For example, silicon changes the mobility of both interstitials and vacancies. FeCrNiTi is a low-carbon alloy, and TiC is not formed. Instead, oversized titanium in austenitic stainless steels reduces the free vacancy concentration due to vacancy trapping by titanium, and reduces the swelling [33, 45, 46]. On the other hand, titanium acts to promote swelling in the cyclic-temperature neutron-irradiation as discussed in Sect. 3.1. Carbon interacts with vacancies and reduces the mobility [47]. However, the formation of metal carbides changes the situation as discussed in Sect. 5.2.

5.2 Formation of precipitates

The effect of phosphorus is easy to understand. The formation of Fe_2P prevents the clustering of point defects because of the high sink efficiency of precipitates for both point defects (Fig. 6). However, although the Ti-added modified 316SS contains 0.024 wt% phosphorus, no Fe_2P was detected by irradiation of 0.29 dpa at 673 K (Fig. 10). Other elements prevent the formation of Fe_2P . The cooperative effects of alloying elements have not been studied sufficiently.

One difference between model alloys and commercial alloys is the existence of carbon in commercial alloys. Even SUS316L contains carbon of 0.019 wt%. Metal carbides, commonly formed by the irradiation of austenitic stainless

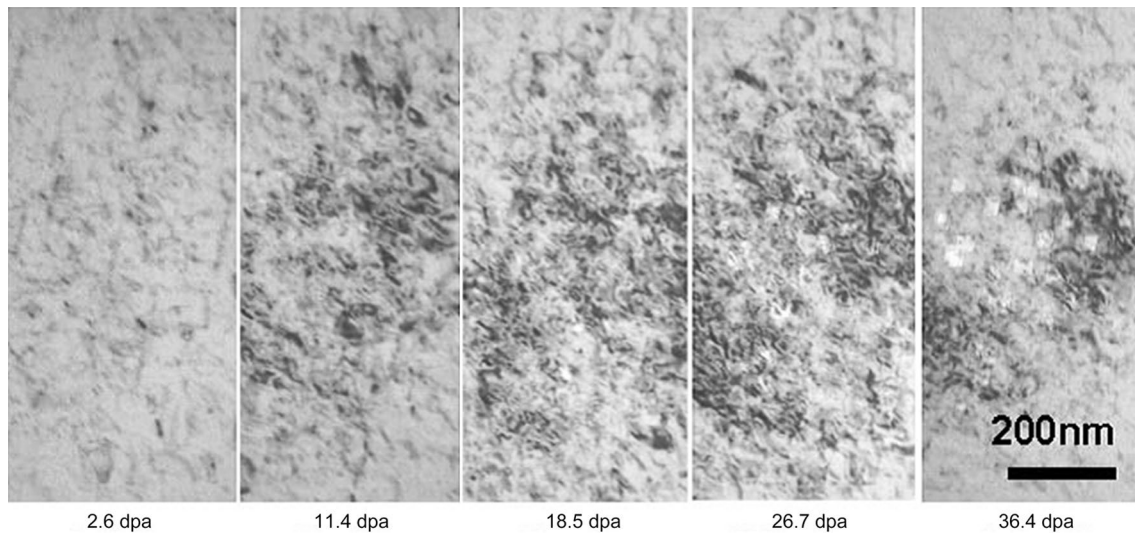


Fig. 18 Damage structure of Ti-added modified 316SS irradiated and observed by high-voltage TEM of 2 MeV at 723 K. The magnifications of all photos are the same

Table 4 Void swelling of JPCA

Temperature (K)	Damage (dpa)	Void radius (nm)	Number Density (m^{-3})	Swelling	Reactor	References
573	33.6	1.5	1.9×10^{23}	2.3×10^{-1}	HFIR	[14]
613	10.5	0.6	1.9×10^{23}	1×10^{-2}	HFIR	[13]
643	6.7	3.1	1.2×10^{21}	2.3×10^{-2}	FFTF	[10]
663	23.5	6.5	1.27×10^{21}	1.65×10^{-1}	FFTF	[15]
663	39.2	6.95	1.71×10^{21}	3.33×10^{-1}	FFTF	[15]
673	4.2	0.22	8×10^{22}	3×10^{-4}	JOYO	This work
673	7.4	3	9×10^{21}	3×10^{-2}	ORR ^a	[34]
673	10.0	6.0	2.9×10^{23}	8×10^{-2}	HFIR	[13]
673	17.3	1.5	1.1×10^{22}	1.6×10^{-2}	ORR + HFIR	[35]
673	34.0	1.3	2.9×10^{23}	2.5×10^{-1}	HFIR	[14]
683	31.5	7.93	1.06×10^{21}	2.7×10^{-1}	FFTF	[15]
683	52.5	6.92	4.24×10^{21}	8.25×10^{-1}	FFTF	[15]
693	40.2	3.1	2.2×10^{21}	4.5×10^{-2}	FFTF	[10]
701	15.0	0.28	8×10^{22}	7×10^{-4}	FFTF	This work
733	23.5	11.1	1.14×10^{20}	7.8×10^{-2}	FFTF	[15]
733	39.2	17.6	7.92×10^{19}	2.05×10^{-1}	FFTF	[15]
763	0.47	0.2	1×10^{23}	4×10^{-4}	JOYO	This work
773	34.5	2.8	1.3×10^{23}	5.1×10^{-1}	HFIR	[14]
793	34.7	26.7	6.7×10^{18}	7.8×10^{-2}	FFTF	[15]
793	40.3	0.72	9.5×10^{20}	2.2×10^{-4}	FFTF	[10]
793	57.8	60.8	4.38×10^{19}	7.64	FFTF	[15]
873	36.5	3.2	1.7×10^{23}	2.2×10^{-1}	HFIR	[14]
873	40.5	0.95	1.2×10^{20}	7.6×10^{-4}	FFTF	[10]

^aThe Oak Ridge National Laboratory Research Reactor

steels, have incoherent grain boundaries with the matrix. Therefore, vacant spaces smaller than single vacancies act as neutral sinks for vacancies and interstitials, and induce recombination between vacancies and interstitials [48]. For the formation of metal carbides, the migration of interstitial carbon is important as well as the accumulation of carbide-former elements such as chromium, molybdenum and titanium by vacancies. Free carbon migrates in the matrix or is trapped at some sites, such as lattice defects. The de-trapping of carbon is induced by irradiation. In 'D', the carbon concentration was less than 0.002% and the formation of TiC was not significant. The lifetime of 140–150 ps in no carbon-containing alloys 'C' and 'D' irradiated by neutrons to 0.2 dpa at 573 K (Fig. 9, right) was that of SFT and loops. Although in commercial alloys, the formation of SFT and loops was expected to be the same as in the model alloys, we concluded that the lifetime of 140–150 ps corresponded to that of precipitates in commercial alloys. TEM identified the formation of metal carbides in JPCA at high temperatures and high irradiation doses [13–15, 27]. However, a strong possibility exists for the formation of TEM unobservable small metal carbides even at a low dose of 1.6×10^{-3} dpa at 573 K, as detected by PALS (Fig. 9b). If the density of metal carbides is high, small precipitates act as an effective sink for both point defects.

6 Start of steady-state void swelling

The high density and small size of micro-voids in JPCA during the incubation period indicate that the alloying elements do not prevent nucleation but prevent the growth of micro-voids, as can be seen in Table 4. Therefore, we can conclude that micro-voids can nucleate but not grow during the incubation period. There are several void swelling mechanisms. According to the dislocation bias theory, the growth of interstitial type dislocation loops is essential [49, 50], which retains the excess vacancies in the matrix to form voids. Alloying elements and precipitates act as the trapping sites of vacancies and interstitials, which reduces the interstitials to contribute to the growth of loops. Alloying elements and precipitates also prevent the one-dimensional motion of interstitial clusters [51, 52], which is the main mechanism of void swelling due to the production bias [53–56]. The addition of alloying elements and precipitates prevents the replacement collision sequence. In cascade, a vacancy-rich area is surrounded by an interstitial-rich area. The geometrical difference between these two areas decreases with the shortening of the length of the replacement collision sequence. Consequently, the mutual annihilation rate of the point defects increases. At the same time, one of the void swelling mechanisms, the cascade localization induced bias

effect, originating from the difference of point defect initial distribution in cascades, does not work effectively [57–60].

After prolonged irradiation, the restriction condition for void swelling is released and the void swelling starts. The completion of precipitation (the coalescence of precipitates, and the dissolution of precipitates [14]), the irradiation-induced segregation of alloying elements, and the purification of the matrix play important roles in the initiation of steady-state void swelling. For example, the role of silicon and carbon in reducing point defect mobility is diminished by the formation of Ni_3Si and metal carbides, respectively. However, in the case of carbon, metal carbides also act as effective sinks for point defects. The total sink strength of metal carbides for point defects, however, decreases with the growth of carbides, which induces void swelling [15, 37]. The saturation of dislocation density after the growth of interstitial type dislocation loops and the accumulation of helium in vacancies [1, 61] are also important factors for the start of void swelling. The saturation of dislocation density determines the destination of point defects, which is interstitials to dislocations and vacancies to voids (dislocation bias mechanism). The irradiation and observation by high-voltage TEM clearly showed void growth after dislocation development (Fig. 18). The difference between electron irradiation and neutron irradiation is the formation of cascade damages. Even in neutron irradiation, the cascade size differs between 14 MeV neutrons and fission neutrons. But in the present studies, we did not discuss this point. The cascade size affects the one-dimensional migration of interstitial clusters and the cascade localization induced bias effect, and consequently the void swelling. But in our studies, the effect of cascade size was not significant and only the total damage (dpa) was the main parameter. The production of helium by nuclear reactions is a serious problem in nuclear materials, especially fusion reactor materials. The vacancies trapped by helium decrease the mobility and promote the nucleation of micro-voids. Further accumulation of helium in vacancy clusters plays an important role in bubble formation, but we do not discuss it further.

7 Conclusion and future studies required

This manuscript reported the defect structures in the incubation period of void swelling in austenitic stainless steels and their model alloys under various irradiation conditions taking advantage of both PALS and TEM. We emphasized the application of PALS for very small vacancy type clusters which are difficult for TEM. Our conclusion is that the incubation period is determined mainly by the alloying elements. We also studied the point defect processes during the incubation periods in ferritic stainless steels, and almost the same conclusion was obtained [62, 63]. So, our

results in austenitic stainless steels will be applicable for the alloy design of improved radiation tolerant metals and alloys such as tungsten and oxide dispersion-strengthened alloys for fusion reactor materials.

To understand the incubation period of void swelling, the detection of microscopic precipitation and segregation is important as well as defect structures. Precipitates were only observed by conventional TEM in our studies, but the resolution was not sufficient. More advanced TEM techniques such as electron energy-loss spectroscopy, energy dispersive X-ray spectroscopy and Z-contrast of high-angle annular dark-field (HAADF) imaging [64] are necessary for these studies. Atom probe tomography is one of the best methods to identify the size and elements of nano-scale precipitates [65]. Even using positrons, AMOC (age-momentum correlation) method is the combination of PALS and Doppler broadening of positron annihilation radiation, and makes it possible to identify the elements where positrons annihilated [66]. More microscopic information will be required for further understanding of void swelling.

Austenitic stainless steels are important nuclear materials due to their excellent properties. But if we consider the decommissioning of the nuclear power plants, a disadvantage is the generation of long-life residual activation in molybdenum and nickel. To reduce these elements is an important task for alloy design. One proposal is to interchange molybdenum with tungsten [67], and the other is nickel and molybdenum with manganese and silicon [68]. Tungsten is commonly used in steels as a ferrite former and not so much in austenitic steels. But tungsten contributes to form small precipitates in steels, which could possibly lead to reduced void-swelling. Further alloy developments are required for successful application of austenitic stainless steels as nuclear materials for high-dose applications.

References

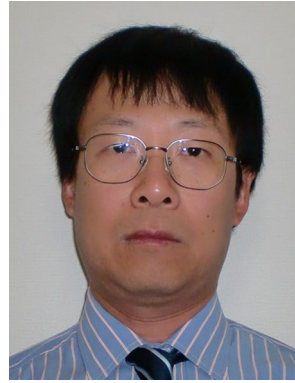
- Mansur LK, Coghlan WA. Mechanisms of helium interaction with radiation effects in metals and alloys: a review. *J Nucl Mater.* 1983;119(1):1.
- Stoller RE, Golubov SI, Domain C, Becquart CS. Mean field rate theory and object kinetic Monte Carlo: a comparison of kinetic models. *J Nucl Mater.* 2008;382(2–3):77.
- Surh MP, Sturgeon JB, Wolfer WG. Void nucleation, growth, and coalescence in irradiated metals. *J Nucl Mater.* 2008;378(1):86.
- Garner FA. Recent insights on the swelling and creep of irradiated austenitic alloys. *J Nucl Mater.* 1984;122–123(1–3):459.
- Kim H, Gigax JG, Fan J, Garner FA, Sham TL, Shao L. Swelling resistance of advanced austenitic alloy A709 and its comparison with 316 stainless steel at high damage levels. *J Nucl Mater.* 2019;527:151818.
- Brandt W, Dupasquier A, editors. *Positron Solid-State Physics.* North-Holland Pub. Co.; 1983.
- Schultz PJ, Lynn KG. Interaction of positron beams with surfaces, thin films, and interfaces. *Rev Mod Phys.* 1988;60(3):701.
- Yoshiie T, Satoh Y, Xu Q. Analysis of defect structural evolution in fcc metals irradiated with neutrons under well defined boundary conditions. *J Nucl Mater.* 2004;329–333(A):81.
- Yoshiie T, Xu Q, Satoh Y, Ohkubo H, Kiritani M. The effect of alloying elements on the defect structural evolution in neutron irradiated Ni alloys. *J Nucl Mater.* 2000;283–287(1):229.
- Kohno Y, Kohyama A, Kayano H. Microstructural evolution of titanium modified austenitic stainless steel after FFTF irradiation. *J Nucl Mater.* 1992;191–194(B):742.
- Hasiguti RR. Japanese program of materials research for fusion reactors. *J Nucl Mater.* 1981;103:51.
- Furuya K, Shiraishi H, Tanaka M. The endurance limit of JACA alloy at 703 K in vacuum. *J Nucl Mater.* 1985;133–134:853.
- Tanaka MP, Maziasz PJ, Hishinuma A, Hamada S. Microstructural development of PCAs irradiated in HFIR at 300 to 400 °C. *J Nucl Mater.* 1986;141–143(2):943.
- Tanaka MP, Hamada S, Hishinuma A, Maziasz PJ. Microstructural development of austenitic stainless steels irradiated in HFIR. *J Nucl Mater.* 1988;155–157(2):801.
- Katoh Y, Kohno Y, Kohyama A. Microstructural response of titanium-modified austenitic stainless steels to neutron exposure of 70 dpa in FFTF/MOTA. *J Nucl Mater.* 1994;212–215(1):464.
- Vevea BJ, McClintock DA, Hyres JW, Riemer BW. Characterization of irradiated AISI 316L stainless steel disks removed from the Spallation Neutron Source. *J Nucl Mater.* 2014;450(1–3):147.
- Wakui T, Wakai E, Naoe T, Shintaku Y, Li T, Murakami K, Kanomata K, Kogawa H, Haga K, Takada H, Futakawa M. Recent studies for structural integrity evaluation and defect inspection of J-PARC spallation neutron source target vessel. *J Nucl Mater.* 2018;506:3.
- Kurata Y. Corrosion experiments and materials developed for the Japanese HLM systems. *J Nucl Mater.* 2011;415(3):254.
- Muroga T, Miyamoto Y, Watanabe H, Yoshida N. Defect accumulation in JPCA and its high purity model alloys irradiated with D-T neutrons. *J Nucl Mater.* 1988;155–157(2):810.
- Watanabe H, Muroga T, Yoshida N. The temperature dependent role of phosphorus and titanium in microstructural evolution of Fe–Cr–Ni alloys irradiated in FFTF. *J Nucl Mater.* 1996;228(3):261.
- Yoshida N, Xu Q, Watanabe H, Muroga T, Kiritani M. Low dose fission neutron irradiation on P- and Ti-modified austenitic alloys with improved temperature control austenitic alloys with improved temperature control. *J Nucl Mater.* 1992;191–194(B):1114.
- Horiki M, Yoshiie T, Huang SS, Sato K, Cao XZ, Xu Q, Troev TD. Effects of alloying elements on defect structures in the incubation period for void swelling in austenitic stainless steels. *J Nucl Mater.* 2013;442(1–3):5813.
- Horiki M, Yoshiie T, Sato K, Xu Q. Point defect processes in neutron irradiated Ni, Fe–15Cr–16Ni and Ti-added modified SUS316SS. *Phil Mag.* 2013;93(14):1701.
- Yoshiie T, Hayashi Y, Yanagita S, Xu Q, Satoh Y, Tsujimoto H, Kozuka T, Kamae K, Mishima K, Shiroya S, Kobayashi K, Utsuro U, Fujita YA. New materials irradiation facility at the Kyoto University Reactor. *Nucl Inst Meth Pys Res A.* 2003;498(1–3):522.
- Hirsch PB, Howie A, Nicholson RB, Pashley DW, Whelan MJ. *Electron microscopy of thin crystals.* Butterworths; 1965.
- Kirkegaard P, Olsen JV, Eldrup M, Pedersen NJ. PALSfit: A computer program for analysing positron lifetime spectra. Roskilde: Technical University of Denmark; 2009.
- Yoshiie T, Cao XZ, Sato K, Miyawaki K, Xu Q. Point defect processes during incubation period of void growth in

- austenitic stainless steels, Ti-modified 316SS. *J Nucl Mater.* 2011;417(1–3):968.
28. Shivachev BL, Troev T, Yoshiie T. Positron lifetime computations of defects in nickel containing hydrogen or helium. *J Nucl Mater.* 2002;306(2–3):105.
 29. Kuramoto E, Tsutsumi T, Ueno K, Ohmura M, Kamimura Y. Positron lifetime calculations on vacancy clusters and dislocations in Ni and Fe. *Comp Mater Sci.* 1999;14(1–4):28.
 30. Satoh Y, Taoka H, Kojima S, Yoshiie T, Kiritani M. Diffraction contrast images of small stacking fault tetrahedra in fcc metals. *Philos Mag.* 1994;A70(5):869.
 31. Yoshida N, Xu Q, Watanabe H, Miyamoto Y, Muroga T. Effect of cyclic temperature change on microstructural evolution in austenitic stainless steels under fission neutron irradiation. *J Nucl Mater.* 1994;212–215(1):471.
 32. Kiritani M, Endoh T, Hamada K, Yoshiie T, Okada A, Kojima S, Satoh Y, Kayano H. Fission reactor irradiation of materials with improved control of neutron flux-temperature history. *J Nucl Mater.* 1991;179–181(2):1104.
 33. Kato T, Takahashi H, Izumiya M. Effects of systematic modification with oversized elements on void formation in 316L austenitic stainless steel under electron irradiation. *Mater Trans JIM.* 1991;32(10):921.
 34. Sawai T, Maziasz PJ, Kanazawa H, Hishinuma A. Microstructural evolution of welded austenitic stainless steels irradiated in the spectrally-tailored ORR experiment at 400°C. *J Nucl Mater.* 1992;191–194(B):712.
 35. Hashimoto N, Wakai E, Robertson JP, Sawai T, Hishinuma A. Microstructure of austenitic stainless steels irradiated at 400°C in the ORR and the HFIR spectral tailoring experiment. *J Nucl Mater.* 2000;280(2):186.
 36. Hamada S, Maziasz PJ, Tanaka MP, Suzuki M, Hishinuma A. Temperature dependence of swelling in type 316 stainless steel irradiated in HFIR. *J Nucl Mater.* 1988;155–157(2):838.
 37. Hamada S, Suzuki M, Maziasz PJ, Hishinuma A. Microstructural evolution in austenitic stainless steels irradiated to 57 dpa in HFIR. *J Nucl Mater.* 1991;179–181(1):515.
 38. Kiritani M, Yoshiie T, Kojima S, Satoh S. Recoil energy spectrum analysis and impact effect of cascade and subcascade in 14 MeV D-T fusion neutron irradiated fcc metals. *Radiat Effect Defect Solid.* 1990;113(1–3):75.
 39. Shimomura Y, Fukushima H, Kami K, Yoshiie T, Yoshida H, Kiritani M. Thermal stability of cascade defects in fcc pure metals. *J Nucl Mater.* 1986;141–143(2):846.
 40. Puska MJ, Nieminen RM. Defect spectroscopy with positrons - a general calculational method. *J Phys.* 1983;F13(2):333.
 41. Yoshiie T, Hasegawa M, Kojima S, Sato K, Saito H, Yamaguchi S, Kiritani M. Positron lifetime measurement and latent vacancy clusters in 14 MeV neutron irradiated nickel. *J Nucl Mater.* 1991;179–181(2):931.
 42. Kinoshita H, Watanabe S, Mochizuki S, Sakaguchi N, Takahashi H. Effect of Ni and Cr concentration on grain boundary segregation in Fe–Cr–Ni alloys. *J Nucl Mater.* 1996;239:205.
 43. Mansur LK, Yoo MH. The effects of impurity trapping on irradiation-induced swelling and creep. *J Nucl Mater.* 1978;74(2):228.
 44. Porollo SI, Shulepin SV, Konobeev YV, Garner FA. Influence of silicon on swelling and microstructure in Russian austenitic stainless steel EI-847 irradiated to high neutron doses. *J Nucl Mater.* 2008;378(1):17.
 45. Sekio Y, Yamashita S, Sakaguchi N, Takahashi H. Void denuded zone formation for Fe–15Cr–15Ni steel and PNC316 stainless steel under neutron and electron irradiations. *J Nucl Mater.* 2015;458:355.
 46. Yabuuchi A, Maekawa M, Kawasuso A. Influence of oversized elements (Hf, Zr, Ti and Nb) on the thermal stability of vacancies in type 316L stainless steel. *J Nucl Mater.* 2012;430(1–3):190.
 47. Kiritani. Nature of point defects and their interactions revealed by electron-microscope observation of their clusters. In: Takamura JI, Doyama M, Kiritani M, editors. *Yamada conference V, Point defects and defect interactions in metals.* Tokyo:University of Tokyo Press; 1982. p. 59.
 48. David C, Panigrahi BK, Balaji S, Balamurugan AK, Nair KGM, Amarendra G, Sundar CS, Raj B. A study of the effect of titanium on the void swelling behavior of D9 steels by ion beam simulation. *J Nucl Mater.* 2008;383(1–2):132.
 49. Greenwood GW, Foreman AJE, Rimmer DE. The role of vacancies and dislocations in the nucleation and growth of gas bubbles in irradiated fissile materials. *J Nucl Mater.* 1959;1(4):305.
 50. Brailsford AD, Bullough R. The rate theory of swelling due to void growth in irradiated metals. *J Nucl Mater.* 1972;44(2):121.
 51. Foreman AJE, English CA, Phythian WJ. Molecular dynamics calculations of displacement threshold energies and replacement collision sequences in copper using a many-body potential. *Philos Mag A.* 1992;66(5):655.
 52. Kuramoto E. Computer simulation of fundamental behaviors of interstitial clusters in Fe and Ni. *J Nucl Mater.* 2000;276(1–3):143.
 53. Woo CH, Singh BN. The concept of production bias and its possible role in defect accumulation under cascade damage conditions. *Phys Status Solidi B.* 1990;159(2):609.
 54. Woo CH, Singh BN. Production bias due to clustering of point defects in irradiation-induced cascades. *Philos Mag A.* 1992;65(4):889.
 55. Singh BN, Trinkaus H, Woo CH. Production bias and cluster annihilation: Why necessary? *J Nucl Mater.* 1994;212–215(1):168.
 56. Golubov SI, Singh BN, Trinkaus H. Defect accumulation in fcc and bcc metals and alloys under cascade damage conditions - Towards a generalisation of the production bias model. *J Nucl Mater.* 2000;276(1–3):78.
 57. Yoshiie T, Satoh Y, Kojima S, Kiritani M. Effect of cascade localization induced bias on defect structure evolution. *J Nucl Mater.* 1991;179–181(2):954.
 58. Yoshiie T, Kiritani M. Cascade localization induced bias effect for void growth. *Mater Sci Forum.* 1992;97–99:105.
 59. Yoshiie T, Kiritani M. The Variation of cascade localization induced bias effect with material parameters and irradiation conditions. *J Nucl Mater.* 1992;191–194(B):1088.
 60. Yoshiie T, Kiritani M. Effect of cascade localization induced bias effect and fluctuation of point defect reactions on defect structure evolution near planar sinks. *J Nucl Mater.* 1994;212–215(1):315.
 61. Hayns MR, Wood MH, Bullough R. A theoretical evaluation of dual-beam irradiation experiments. *J Nucl Mater.* 1978;75(2):241.
 62. Huang SS, Pan XQ, Sato K, Xu Q, Yoshiie T. Early stage irradiation effects in F82H model alloys. *J Nucl Mater.* 2014;449(1–3):248.
 63. Huang SS, Xu Q, Yoshiie T. Effects of Cr and W on defects evolution in irradiated F82H model alloys. *Mater Lett.* 2016;178:272.
 64. Midgley PA, Weyland M. 3D electron microscopy in the physical sciences: the development of Z-contrast and EFTEM tomography. *Ultramicroscopy.* 2003;96(3–4):413.
 65. Kelly TF, Miller MK. Atom probe tomography. *Rev Sci Instrum.* 2007;78(3):031101.
 66. Seeger A. Challenges to positron and positronium physics by materials science. *Mater Sci Forum.* 1997;255–257:1.
 67. Salama E, Eissa MM, Tageldin AS. Distinct properties of tungsten austenitic stainless alloy as a potential nuclear engineering material. *Nucl Eng Tech.* 2019;51(3):784.
 68. Weber S, Martin M, Theisen W. Lean-alloyed austenitic stainless steel with high resistance against hydrogen environment embrittlement. *Mater Sci Eng A.* 2011;528(25–26):7688.



Dr. Toshimasa Yoshiie is an emrtitus professor of Kyoto University. He works currently as a researcher in the Institute for Integrated Radiation and Nuclear Science, Kyoto University. He received a doctorate of engineering from Osaka University in 1977. He had worked in Nagasaki University, Carnegie Mellon University, Hokkaido University and Kyoto University. His research intersts include lattice defects and irradiation effects in materials. He has published over

250 papers in peer reviewed journals. He is a member of International Adversory Board in COSIRES (Computer Simulation of Irradiation Effects in Solids) Committee.



Dr. Xu Qiu is an associate profes-
sor at the Institute for Integrated
Radiation and Nuclear Science,
Kyoto University. He graduated
from Kyushu University in Japan
with a doctorate in engineering
in 1995. Then, he joined the
Kyoto University Research Reac-
tor Institute as an assistant pro-
fessor. He has long been engaged
in basic research on the interac-
tion of materials with high
energy particles (neutrons, ions,
electrons). He published more
than 250 articles in *Scientific
Reports*, *Nanotechnology*,

Nuclear Fusion, *Phys. Rev. B.*, *Phys. Rev. C.*, *Appl. Phys. Lett.*, *Phil. Mag. Lett.*, *Acta Mater.* and *Journal of Nuclear Materials*, and so on. He is an editorial board member of *Scientific Reports*.